Ellipsoidal statistical Bhatnagar–Gross–Krook model with velocity-dependent collision frequency

Yingsong Zheng[a)]
Department of Mechanical Engineering, University of Strathclyde, Glasgow G1 1XJ, United Kingdom

Henning Struchtrup[b)]
Department of Mechanical Engineering, University of Victoria, Victoria, British Columbia V8W 3P6, Canada

(Received 11 June 2005; accepted 25 October 2005; published online 15 December 2005)

In this paper, an ellipsoidal statistical (ES) Bhatnagar–Gross–Krook (BGK)-type kinetic model with velocity-dependent collision frequency is proposed and further numerically tested for one-dimensional shock waves and planar Couette flow at steady state for hard sphere molecules. In this new kinetic model, a physically meaningful expression for the velocity-dependent collision frequency derived from the Boltzmann equation is used, while the important properties for a kinetic model are retained at the same time. This kinetic model can be simplified to the classical ES-BGK model and the BGK model with velocity-dependent collision frequency for suitable choices of parameters. The H theorem for this new kinetic model has so far been proven only for small Knudsen numbers. The numerical method used here for kinetic models is based on Mieussens's discrete velocity model [L. Mieussens, J. Comput. Phys. **162**, 429 (2000)]. Computational results from the kinetic models (including the BGK model, the ES-BGK model, the BGK model with velocity-dependent collision frequency, and this new kinetic model) are compared to results obtained from the direct simulation Monte Carlo (DSMC) method. It is found that results obtained from this new kinetic model lie in between results from the ES-BGK model and results from the BGK model with velocity-dependent collision frequency. For one-dimensional shock waves, results from this new kinetic model fit best with results from the DSMC, while for planar Couette flow, the classical ES-BGK model is suggested. © *2005 American Institute of Physics*.
[DOI: 10.1063/1.2140710]

I. INTRODUCTION

Processes in rarefied gases must be described through the Boltzmann equation, which is a nonlinear integrodifferential equation. Since the Boltzmann equation is difficult to handle, and its numerical solution is time expensive, some alternative, simpler expressions have been proposed to replace the Boltzmann collision term. These are known as collision models, and any Boltzmann-like equation where the Boltzmann collision integral is replaced by a collision model is called a model equation or a kinetic model.[1–5]

A good kinetic model should be easier to use than the Boltzmann equation, but should at the same time mimic the behavior of the Boltzmann equation closely. The best known kinetic model is the Bhatnagar–Gross–Krook model (BGK model),[1,3–6] which already fails in the description of a dense gas (i.e., at small Knudsen numbers), since it yields a wrong value for the dimensionless ratio of viscosity and heat conductivity, which is known as the Prandtl number. Other kinetic models were introduced in order to overcome that deficiency, including the ellipsoidal statistical BGK model (ES-BGK model),[3–5,7–9] the BGK model with velocity-dependent collision frequency [$\nu(C)$-BGK model],[10–16] the Shakhov model,[17,18] and the Liu model.[19,20] While all of these yield the proper Prandtl number, the results obtained from them differ from results obtained from the full Boltzmann equation as the gas becomes rarefied.

All kinetic models require the collision frequency of a particle as a parameter. A study of the Boltzmann equation shows that the collision frequency is a function of the particle speed—fast particles collide more often—and the details of the behavior of a rarefied gas will depend on the collision frequency.[1,3] This implies also that the quality of a kinetic model will depend on its ability to incorporate the proper–velocity-dependent expression for the collision frequency.

In this paper we propose a new kinetic model that allows us for the first time to incorporate the proper expression for the collision frequency for an arbitrary molecular model. This new model combines ideas from the ES-BGK model, which requires a velocity-independent collision frequency, and the $\nu(C)$-BGK model, in which the use of the proper collision frequency yields a wrong value for the Prandtl number.

After the new kinetic model is constructed, numerical tests of this new and some existing kinetic models are done for one-dimensional shock waves at steady state and planar Couette flow at steady state, which are two important bench-

a)Telephone: 44-141-548-4497. Fax: 44-141-552-5105. Electronic mail: yingsong.zheng@strath.ac.uk
b)Telephone: 1-250-721-8693. Fax: 1-250-721-6051. Electronic mail: struchtr@me.uvic.ca

mark problems for rarefied gas flows. Further, results are compared with results from the direct simulation Monte Carlo (DSMC) solutions of the Boltzmann equation.[21] (Based on Bird's code, which is available in the public domain.[22]) The numerical method used here is Mieussens's discrete velocity model (DVM),[11,23–25] which has been applied before to the BGK model, the ES-BGK model and the $\nu(C)$-BGK model. The computational results show that indeed the incorporation of the velocity-dependent collision frequency (from now on abbreviated as VDCF) leads to better agreement between kinetic models and Boltzmann equation.

II. KINETIC THEORY, KINETIC MODELS, AND PROPERTIES OF THE COLLISION TERM

In the microscopic theory of rarefied gasdynamics, the state variable is the distribution function $f(\mathbf{x},\mathbf{c},t)$,[26] which specifies the density of microscopic particles with velocity $\mathbf{c}$ at time t and position $\mathbf{x}$. The particles, which can be thought of as idealized atoms, move freely in space unless they undergo collisions. The corresponding evolution of f is described by the Boltzmann equation,[1–3] which, when external forces are omitted, is written as

$$\frac{\partial f}{\partial t} + c_i \frac{\partial f}{\partial x_i} = S(f). \tag{1}$$

Here, the first term on the left-hand side describes the local change of f with time and the second term is the convective change of f due to the microscopic motion of the gas particles. The term on the right-hand side, $S(f)$, describes the change of f due to collisions among particles.

In the macroscopic continuum theory of rarefied gasdynamics, the state of the gas is described by macroscopic variables, such as mass density ρ, macroscopic flow velocity $\mathbf{u}$, temperature T, and so on, which depend on position $\mathbf{x}$ and time t. These quantities can be recovered from the distribution f by taking velocity averages (moments) of the corresponding microscopic quantities, such as

$$\begin{aligned}
&\rho = \int f\, d\mathbf{c}, \quad \rho u_i = \int c_i f\, d\mathbf{c},\\
&\rho e = \frac{3}{2}p = \frac{3}{2}\rho RT = \int \frac{1}{2}C^2 f\, d\mathbf{c},\\
&p_{ij} = \int f C_i C_j\, d\mathbf{C} = p\,\delta_{ij} + \sigma_{ij}, \quad \sigma_{ij} = \int f C_{<i} C_{j>}\, d\mathbf{c},\\
&q_i = \frac{1}{2}\int C^2 C_i f\, d\mathbf{c},
\end{aligned} \tag{2}$$

where ρe is the density of internal energy, $R=k/m$ is the gas constant, m is the mass of one microscopic particle, k is the Boltzmann constant, $\mathbf{C}=\mathbf{c}-\mathbf{u}$ is the peculiar velocity (therefore, $g=|\mathbf{c}-\mathbf{c}^1|=|\mathbf{C}-\mathbf{C}^1|$, $d\mathbf{c}=d\mathbf{C}$), p is the hydrostatic pressure, p_{ij} is the pressure tensor, σ_{ij} is the trace-free part of the pressure tensor (about the computation of symmetric and trace-free tensors, please refer to Ref. 1) q_i is the heat flux. The third expression of Eqs. (2) gives the definition of temperature from the ideal gas law.

In kinetic models, the Boltzmann collision term $S(f)$, is replaced by a relaxation expression that is typically of the form

$$S_m(f) = -\nu(f - f_{\mathrm{ref}}). \tag{3}$$

Here, f_{ref} is a suitable reference distribution function, and ν is the (mean) collision frequency; the various kinetic models differ in their choices for f_{ref} and ν.

Any collision model $S_m(f)$ needs to retain the main properties satisfied by the Boltzmann collision integral, which are as follows:[3,11,27,28]

(1) It guarantees the conservation of mass, momentum, and energy, which are

$$\int S_m\, d\mathbf{c} = 0, \quad \int c_i S_m\, d\mathbf{c} = 0, \quad \frac{1}{2}\int c^2 S_m\, d\mathbf{c} = 0. \tag{4}$$

(2) The production of entropy χ is always positive (H theorem),

$$\chi = -k\int \ln f S_m\, d\mathbf{c} \geqslant 0. \tag{5}$$

(3) In equilibrium, $S_m(f_E)=0$, and therefore, the equilibrium distribution f_E is equal to the Maxwellian distribution f_{M}, given by

$$f_{\mathrm{M}} = \frac{\rho}{m}\sqrt{\left(\frac{1}{2\pi RT}\right)^3}\exp\left(-\frac{C^2}{2RT}\right). \tag{6}$$

(4) In the hydrodynamic limit $S_m(f)$ yields the right transport coefficients, such as viscosity μ, thermal conductivity κ, and Prandtl number $\mathrm{Pr}=(5R/2)(\mu/\kappa)$. The Prandtl number is close to 2/3 for all physically meaningful collision factors σ; $\mathrm{Pr}\cong 2/3$ for ideal monatomic gas is also found in experiments.[29]

(5) The collision term $S_m(f)$ depends on the peculiar velocity $\mathbf{C}=\mathbf{c}-\mathbf{u}$, and not the microscopic velocity $\mathbf{c}$, since the Boltzmann equation is invariant under Galilean transformation.

(6) The resulting transport equation predicts positive distributions f in any situation.

III. EXPRESSIONS FOR THE COLLISION FREQUENCY

The collision frequency for an ideal gas in thermal equilibrium is given by[1,2,30]

$$\nu(x_i,t,C_i) = \int f_M^1 \sigma g \sin\theta\, d\theta\, d\varepsilon\, d\mathbf{c}^1, \tag{7}$$

where the superscript 1 denotes parameters for particle 1, which is the collision partner of the particle considered, $g=|\mathbf{c}-\mathbf{c}^1|$ is the relative speed of the colliding particles, σ is the scattering factor, and ε and θ are the angles of collision.

The further evaluation of the collision frequency depends on the interaction potential between the particles. In the following we shall consider inverse power potentials between particles,[1,3,11] of the general form $\phi \sim r^{-(n-1)}$. Here, ϕ

denotes the interaction potential, r is the distance between particles, and $n>3$ gives the order of the potential; $n=5$ represents Maxwell molecules, and $n\to\infty$ describes hard sphere molecules. It can be shown that[1]

$$\sigma g = g^{n-5/n-1}F(\theta), \tag{8}$$

where the function $F(\theta)$ depends only on the collision angle. After some manipulation follows, the physically meaningful expression of the VDCF as

$$\nu(n,\eta) = 2\hat{\nu}_0(n)\frac{\rho}{\sqrt{\pi}}(2RT)^{n-5/2(n-1)}\frac{n-1}{3n-7}\int_0^\infty \frac{\xi e^{-\xi^2}}{\eta} \times[(\xi+\eta)^{3n-7/n-1} - |\xi-\eta|^{3n-7/n-1}]d\xi, \tag{9}$$

where $\hat{\nu}_0(n)=\int F(\theta)\sin\theta\, d\theta\, d\varepsilon$ is a constant that depends on the interaction potential, but is independent of the macroscopic gas properties; $\xi=C^1/\sqrt{2RT}$ and $\eta=C/\sqrt{2RT}$ are dimensionless peculiar velocities.

We also introduce the dimensionless collision frequency in this work as

$$\hat{\nu}(n,\eta) = \frac{\mu}{p}\nu(n,\eta). \tag{10}$$

The mean collision frequency is obtained as[1]

$$\overline{\nu}(n) = \frac{p}{\mu}\bar{\bar{\nu}} = \frac{\int \nu f_M\, dc}{\int f_M\, dc} = \cdots = \overline{\nu}_0(n)\rho(RT)^{n-5/2(n-1)}, \tag{11}$$

where $\overline{\nu}_0(n)$ is a constant and $\bar{\bar{\nu}}$ is the dimensionless mean collision frequency.

Note that the collision frequencies introduced in this section rely on the use of the Maxwellian, which is the equilibrium distribution function. Accordingly, their use in nonequilibrium processes will introduce some inaccuracy, which, however, should be small for up to moderate deviations from equilibrium, and would be unacceptably large for strong deviations from equilibrium. This issue can be seen from the computational results for the planar Couette flow in the later part.

IV. EXISTING KINETIC MODELS

Several kinetic models have been proposed and developed in the past. The best known models are the BGK model,[3–6] the ES-BGK model,[3–5,7–9] the $\nu(C)$-BGK model,[10–16] the Shakhov model,[17,18] and the Liu model.[19,20] These models will be briefly described and compared in this section. Table I shows their basic properties, in particular, whether the models fulfill requirements 1–6 of Sec. II. The kinetic models discussed here are all of the form of Eq. (3).

The BGK model[3,4] is the original and simplest kinetic model, where the reference distribution function is simply the Maxwellian,

$$f_{\text{ref}} = f_M, \tag{12}$$

and its evaluation in the hydrodynamic limit yields (e.g., see Ref. 1)

$$\mu = \frac{p}{\nu}, \quad \kappa = \frac{5}{2}\frac{pR}{\nu}, \quad \text{Pr} = 1. \tag{13}$$

This model is widely used for theoretical considerations, but it violates the requirement (4) of Sec. II, since it gives the wrong value Pr=1 for the Prandtl number. All models described below were introduced to correct this failure.

The ES-BGK model[3–5,7–9] replaces the Maxwellian with a generalized Gaussian, so that

$$f_{\text{ref}} = f_{\text{ES}} = \rho[\det(2\pi\lambda_{ij})]^{-1/2}\exp(-\tfrac{1}{2}C_i\varepsilon_{ij}C_j), \tag{14}$$

and it yields

$$\mu = \frac{1}{1-b}\frac{p}{\nu}, \quad \kappa = \frac{5}{2}\frac{pR}{\nu}, \quad \text{Pr} = \frac{1}{1-b}. \tag{15}$$

Here, the matrix $\boldsymbol{\lambda}$ is defined as

$$\lambda_{ij} = RT\delta_{ij} + b\sigma_{ij}/\rho = (1-b)RT\delta_{ij} + bp_{ij}/\rho, \tag{16}$$

where b is a number that serves to adjust the Prandtl number, δ_{ij} is the unit matrix, and $\boldsymbol{\varepsilon}$ is the inverse of the tensor $\boldsymbol{\lambda}$. b must be in the interval $[-1/2,1]$ to ensure that λ_{ij} is positive definite, which ensures the integrability of f_{ES}. In this model, the reference distribution f_{ES} is defined by the following ten conditions (the first five conditions are the conservation laws),

$$\int f_{\text{ES}}\, d\mathbf{c} = \rho, \quad \int C_i f_{\text{ES}}\, d\mathbf{c} = 0, \quad \int C_i C_j f_{\text{ES}}\, d\mathbf{c} = \rho\lambda_{ij} = (1-b)p\delta_{ij} + bp_{ij}, \tag{17}$$

which will be used in the later numerical work.

Only recently, Andries *et al.* succeeded in proving the validity of the H theorem for the ES-BGK model,[8] which revived the interest in this model.

The Burnett equations for the ES-BGK model for inverse power potentials have been derived and examined by Zheng and Struchtrup.[9] The ES-BGK Burnett equations are found to be identical to the Burnett equations for the Boltzmann equation only in the case of Maxwell molecules, while the Burnett coefficients exhibit some differences for other interaction types, e.g., hard sphere molecules. The linear stability of the ES-BGK Burnett equations was also discussed in Ref. 9.

The $\nu(C)$-BGK model, or the BGK model with VDCF,[10–16] is an extension of the classical BGK model that allows an incorporation of the VCDF. In Ref. 12, this type of kinetic model was discussed without the explicit form of the collision frequency. In Refs. 13 and 14, the discussion was based on the linearized Boltzmann equation, and the explicit form of the collision frequency was only given for two specific cases: hard sphere molecules (denoted as rigid-sphere molecules in Ref. 13) and the Williams model (the collision frequency is proportional to the magnitude of the velocity). In Refs. 15 and 16, the very hard particle interaction model, which does not correspond to any physical interaction

TABLE I. A comparison of kinetic models.

Kinetic models	BGK model	ES-BGK model	$\nu(C)$-BGK model	Shakhov model	Liu model	New kinetic model
f_{ref} in collision term $S_m(f)$	Eq. (12)	Eq. (14)	Eq. (18)	Eq. (21)	Eq. (23)	Eq. (25)
Collision frequency	Velocity independent		Velocity dependent	Velocity independent		Velocity dependent
Main related references	3, 4, and 6	7–9	11, 13, and 14	17 and 18	19 and 20	5 and 32 and this work
First appear year	1954	1964	1966 (linearized Boltzmann equation+ hard spheres); 1997 (whole Boltzmann equation and arbitrary molecular models)	1968	1990	1979 (linearized Boltzmann equation +hard spheres); 2004 (whole Boltzmann equation and arbitrary molecular models)
Conservation laws	Satisfied					
H theorem	Proved	Proved	Proved	Only proved in the near local equilibrium situations		Only proved in small Knudsen numbers
In equilibrium, $f=f_{\text{M}}$	Yes					
Transport coefficients	Eq. (13)	Eq. (15)	Eq. (19)	Eq. (22)	Eq. (24)	Eq. (30)
Galilean invariance	Satisfied					
Positiveness of f	Satisfied	Satisfied	Satisfied	Possibly not	Not true in some situations	Satisfied
Remarks	Simplest model; f_{ref} is a local isotropic Gaussian	f_{ref} is a local anisotropic Gaussian; can simplify to the BGK model when $b=0$	In order to obtain Pr=2/3, the expression of VDCF does not meet with the physics	N/A	N/A	1. Satisfy the requirements of physically meaningful VDCF and correctly transport coefficients in one kinetic model 2. Can simplify to the ES-BGK model and the $\nu(C)$-BGK model at certain conditions

potential,[15] was applied to obtain the expression of VDCF. In Refs. 10 and 11, the discussion was based on the whole Boltzmann equation and the explicit form of the collision frequency was given for any value of n in the inverse power potential. Here, only a brief description will be given following Refs. 10 and 11, in which the corresponding reference distribution is a shifted Maxwellian,

$$f_{\text{ref}} = f_{\gamma} = a \exp(-\Gamma C^2 + \gamma_i C_i), \tag{18}$$

where the coefficients a, $\Gamma > 0$, $\boldsymbol{\gamma}$ are chosen so as to guarantee the conservation of mass, momentum, and energy as given in Eq. (4). In general situations, the explicit theoretical expressions of a, Γ, $\boldsymbol{\gamma}$ cannot be given, and only numerical

values are obtained from these five constraints. In this model, the transport coefficients must be computed according to

$$\mu = \frac{16p}{15\sqrt{\pi}}\int_0^\infty \frac{\eta^6}{\nu(\eta)} e^{-\eta^2}\, d\eta,$$

$$\kappa = \frac{8pR}{3\sqrt{\pi}}\int_0^\infty \frac{\eta^4(\eta^2-5/2)^2}{\nu(\eta)} e^{-\eta^2}\, d\eta, \tag{19}$$

$$\mathrm{Pr} = \frac{5R}{2}\frac{\mu}{\kappa} = \frac{\displaystyle\int_0^\infty \frac{\eta^6}{\nu(\eta)} e^{-\eta^2}\, d\eta}{\displaystyle\int_0^\infty \frac{\eta^4(\eta^2-5/2)^2}{\nu(\eta)} e^{-\eta^2}\, d\eta}.$$

In principle, the collision frequency $\nu(\eta)$ in the $\nu(C)$-BGK model can be assumed to be any function with two unknown coefficients, which are determined by experimental values of viscosity μ and thermal conductivity κ (or one experimental parameter and the condition $\mathrm{Pr}=2/3$). Some possible expressions of $\nu(\eta)$ can be found in Ref. 11. Here, only one expression, which will be used in the numerical tests, is listed,

$$\hat{\nu} = \frac{\mu}{p}\nu = a(1.0+\gamma\eta^2), \tag{20}$$

with $\hat{\nu}$ the dimensionless collision frequency, and two coefficients $a=0.026\,835\,1$ and $\gamma=14.2724$. However, the proper expression of $\nu(C)$, based on the Boltzmann collision term, Eq. (10), yields $\mathrm{Pr}\approx 1.0$, that is it does not give the proper Prandtl number.[10]

The Shakhov model was proposed by Shakhov,[17,18] and chooses the reference distribution function as

$$f_{\mathrm{ref}} = f_S = f_{\mathrm{M}}\left[1+\frac{2q_iC_i}{15pRT}\left(\frac{C^2}{2RT}-\frac{5}{2}\right)\right]; \tag{21}$$

and it gives

$$\mu = \frac{p}{\nu}, \quad \kappa = \frac{15}{4}\frac{pR}{\nu}, \quad \mathrm{Pr} = \frac{2}{3}. \tag{22}$$

The Liu model was proposed by Liu,[19,20] in which

$$f_{\mathrm{ref}} = f_L = f_{\mathrm{M}}\left[1+\frac{p_{ij}C_{<i}C_{j>}}{2pRT}+\frac{2q_iC_i}{5pRT}A - \frac{\Omega_1^{(2)}(2)}{\nu}\frac{4\rho}{5mpRT}\left(p_{ij}C_{<i}C_{j>}+\frac{8q_iC_i}{15}A\right)\right], \tag{23}$$

where $A=C^2/2RT-5/2$, and

$$\mu = \frac{5}{8}\frac{kT}{\Omega_1^{(2)}(2)}, \quad \kappa = \frac{75}{32}\frac{k^2T}{m\Omega_1^{(2)}(2)}, \quad \mathrm{Pr} = \frac{2}{3}. \tag{24}$$

Here $\Omega_1^{(2)}(2)$ is a coefficient whose value could be found in Refs. 19 and 30.

Since the heat flux q_i is a vector, and the range of the peculiar velocity is $(-\infty,\infty)$, f_S in Eq. (21) and f_L in Eq. (23) will obviously assume negative values for large values of the peculiar velocity. It follows that the distribution function f from these two kinetic models might become negative for some values of the peculiar velocity, and this might lead to unphysical results. Indeed, for the Liu model, this phenomenon was observed in Ref. 20. This is the reason that the Shakhov model and the Liu model are not utilized in the construction of new kinetic models, and also not included in the numerical tests in this work.

V. CONSTRUCTION METHOD FOR THE NEW ES-BGK TYPE KINETIC MODEL WITH VDCF

In the above existing kinetic models, the collision frequency ν is assumed to be an average value, which is not dependent on the velocity $\mathbf{C}$, except for the $\nu(C)$-BGK model. For real gases, as was shown, the collision frequency is a function of the velocity $\mathbf{C}$. The $\mathbf{C}$ dependence of ν has an important influence on the results at large Knudsen numbers, e.g., for $\mathrm{Kn}\geqslant 0.1$, and thus $\nu(C)$ in kinetic models should be close to the value predicted from the Boltzmann equation. However, when the physically meaningful expression of the VDCF, Eq. (9), is used in the $\nu(C)$-BGK model, the Prandtl number is not 2/3, but close to unity.[11]

Here, we propose a new kinetic model, in which the physically meaningful VDCF is applied, while the transport coefficients are predicted correctly, including $\mathrm{Pr}\cong 2/3$. The basic idea is to combine the anisotropic Gaussian of the ES-BGK model and the VDCF of the $\nu(C)$ BGK model to develop a new kinetic model, named as an ES-BGK model with VDCF, or a $\nu(C)$-ES-BGK model. This idea has been applied in Refs. 31 and 32. In Ref. 31, a kinetic model for hard spheres and inelastic collisions of granular gases was considered. In Ref. 32, the discussion was based on the linearized Boltzmann equation, and the explicit form of the VDCF was given only for hard sphere molecules. In this paper, the complete Boltzmann equation with elastic collisions and any value of n in the inverse power potential is considered, so it is a more general work than Refs. 31 and 32.

In this new kinetic model, the collision term $S_m(f)$ is written as

$$S_m(f) = -\boldsymbol{\nu}(C)(f-f_N),$$
$$f_N = a\exp\left(-\tfrac{1}{2}\Gamma\boldsymbol{\varepsilon}_{ij}C_iC_j+\boldsymbol{\gamma}_iC_i\right). \tag{25}$$

Here, the matrix ε_{ij} has the same expression as in the ES-BGK model, i.e., matrix λ_{ij}, the inverse of ε_{ij}, is given by Eq. (16). The coefficients a, $\Gamma>0$, and $\boldsymbol{\gamma}$ are chosen so as to guarantee the conservation of mass, momentum, and energy.[33]

In general situations, explicit expressions of a, Γ, $\boldsymbol{\gamma}$ cannot be given, and only numerical values can be obtained from the five conservation laws, Eq. (4). At small Knudsen numbers, however, approximate explicit expressions for a, Γ, $\boldsymbol{\gamma}$ can be found through the first-order Chapman-Enskog method, and this is described next.

At small Knudsen numbers, any distribution must be close to a Maxwellian distribution, and Taylor expansion

around the Maxwellian leads, when we only keep the zeroth- and first-order terms, to

$$a=\rho\left(\frac{1}{2RT}\right)^{3/2}(1-\hat{a}),\quad \Gamma=1-\hat{\Gamma},\quad \varepsilon_{ij}=\frac{\delta_{ij}}{RT}-\frac{b\sigma_{ij}}{pRT},$$

$$\Gamma\varepsilon_{ij}=\frac{\delta_{ij}}{RT}-\hat{\Gamma}\frac{\delta_{ij}}{RT}-\frac{b\sigma_{ij}}{pRT},\quad \gamma_i=\hat{\gamma}_i, \tag{26}$$

$$f_N\approx f_{\mathrm{M}}\left(1-\hat{a}+\frac{\hat{\Gamma}C^2}{2RT}+\frac{b\boldsymbol{\sigma}_{ij}C_iC_j}{2pRT}+\hat{\boldsymbol{\gamma}}_iC_i\right).$$

Here, values of the undetermined coefficients $\hat{a}$, $\hat{\Gamma}$, and $\hat{\gamma}_i$ are small compared to 1. The value of parameter b must lie in the interval $[-0.5,1]$, which is the same range as b in the ES-BGK model, to ensure the matrix ε_{ij} is positive definite.

After performing the first-order Chapman-Enskog expansion,[1,2,11,30] one finds

$$f=f_N-\frac{f_{\mathrm{M}}}{\boldsymbol{\nu}}\left[\frac{C_iC_j}{RT}\frac{\partial u_{<i}}{\partial x_{j>}}+\frac{C_i}{T}\frac{\partial T}{\partial x_i}\left(\frac{C^2}{2RT}-\frac{5}{2}\right)\right]. \tag{27}$$

This approximate solution fulfills the five conservation laws for *any* distribution f_{NI}, and thus, the coefficients $\hat{a}$, $\hat{\Gamma}$, and $\hat{\gamma}_i$ cannot be determined from these conditions. However, the distribution f must reproduce the first five moments, which are density, velocity, and pressure; see Eqs. (2). It follows that

$$\hat{a}=\hat{\Gamma}=0,\quad \hat{\gamma}_i=\frac{1}{3pT}\frac{\partial T}{\partial x_i}\int\frac{f_{\mathrm{M}}}{\nu}\left(\frac{C^2}{2RT}-\frac{5}{2}\right)C^2\,d\mathbf{c},$$

$$f_N=f_{\mathrm{M}}\left[1+\frac{bC_iC_j}{2pRT}\boldsymbol{\sigma}_{ij}+\frac{C_i}{3pT}\frac{\partial T}{\partial x_i}\int\frac{f_{\mathrm{M}}}{\boldsymbol{\nu}}\left(\frac{C^2}{2RT}-\frac{5}{2}\right)\times C^2\,d\mathbf{c}\right], \tag{28}$$

$$f=f_{\mathrm{M}}\left[1+\frac{bC_iC_j}{2pRT}\sigma_{ij}+\frac{C_i}{3pT}\frac{\partial T}{\partial x_i}\int\frac{f_{\mathrm{M}}}{\nu}\left(\frac{C^2}{2RT}-\frac{5}{2}\right)C^2\,d\mathbf{c}\right]-\frac{f_M}{\nu}\left[\frac{C_iC_j}{RT}\frac{\partial u_{<i}}{\partial x_{j>}}+\frac{C_i}{T}\frac{\partial T}{\partial x_i}\left(\frac{C^2}{2RT}-\frac{5}{2}\right)\right].$$

The pressure tensor and heat flux vector can be readily computed from the above distribution function as

$$\sigma_{ij}=-\frac{1}{1-b}\frac{32p}{15\sqrt{\pi}}\int_0^\infty\frac{\eta^6}{\nu(\eta)}e^{-\eta^2}\,d\eta\times\frac{\partial u_{<i}}{\partial x_{j>}},$$

$$q_i=-\frac{8pR}{3\sqrt{\pi}}\int_0^\infty\frac{\eta^4(\eta^2-5/2)^2}{\nu(\eta)}e^{-\eta^2}\,d\eta\times\frac{\partial T}{\partial x_i}. \tag{29}$$

Therefore, the transport coefficients and the Prandtl number obtained from this kinetic model are

$$\mu=\frac{1}{1-b}\frac{16p}{15\sqrt{\pi}}\int_0^\infty\frac{\eta^6}{\nu(\eta)}e^{-\eta^2}\,d\eta,$$

$$\kappa=\frac{8pR}{3\sqrt{\pi}}\int_0^\infty\frac{\eta^4(\eta^2-5/2)^2}{\nu(\eta)}e^{-\eta^2}\,d\eta, \tag{30}$$

$$\mathrm{Pr}=\frac{5R}{2}\frac{\mu}{\kappa}=\frac{1}{1-b}\frac{\displaystyle\int_0^\infty\frac{\eta^6}{\nu(\eta)}e^{-\eta^2}\,d\eta}{\displaystyle\int_0^\infty\frac{\eta^4(\eta^2-5/2)^2}{\nu(\eta)}e^{-\eta^2}\,d\eta}=\frac{\Lambda}{1-b},$$

where Λ is defined as

$$\Lambda=\frac{\displaystyle\int_0^\infty\frac{\eta^6}{\nu(\eta)}e^{-\eta^2}\,d\eta}{\displaystyle\int_0^\infty\frac{\eta^4(\eta^2-5/2)^2}{\nu(\eta)}e^{-\eta^2}\,d\eta}. \tag{31}$$

A closer examination shows that these results are very similar to the expressions found for the $\nu(C)$-BGK model, Eqs. (19); indeed, the only difference is the factor $1/(1-b)$ in viscosity and Prandtl number.

We combine Eqs. (9), (10), and (30) and, after some manipulation, one finds the following expressions for dimensionless collision frequency in this new kinetic model:

$$\hat{\nu}(n,\eta)=\frac{1}{1-b}\frac{16}{15\sqrt{\pi}}A(n)B(n,\eta), \tag{32}$$

where

$$A(n)=\int_{\eta=0}^\infty\frac{\eta^6e^{-\eta^2}}{B(n,\eta)}d\eta,$$

$$B(n,\eta)=\int_{\xi=0}^\infty\frac{\xi e^{-\xi^2}}{\eta}[(\xi+\eta)^{3n-7/n-1}-|\xi-\eta|^{3n-7/n-1}]d\xi. \tag{33}$$

Especially for hard sphere molecules where $n=\infty$, one finds

$$\hat{\nu}(n=\infty,\eta)=\frac{1}{2}\frac{1}{1-b}\frac{16}{15\sqrt{\pi}}\cdot A(n=\infty)B(n=\infty,\eta=0.0)\times\left[e^{-\eta^2}+\frac{\sqrt{\pi}}{2}\left(\frac{1}{\eta}+2\eta\right)\mathrm{erf}(\eta)\right], \tag{34}$$

which is the same expression as in Refs. 11, 13, and 30, where

TABLE II. Several n and corresponding b and Pr values for the new kinetic model.

				$b=-0.5$	
n	ω	Λ	b for Pr=2/3	Pr	$\frac{\lvert \mathrm{Pr}-2/3\rvert}{2/3}$
5	1	1.0	−0.50	2/3=0.6667	0.000
6	0.9	1.00839	−0.5126	0.6723	0.008
231.0/31.0	0.81	1.01327	−0.5199	0.6755	0.013
10	0.72	1.01572	−0.5236	0.6771	0.016
13	0.67	1.01615	−0.5242	0.6774	0.016
20	0.61	1.01566	−0.5235	0.6771	0.016
∞	0.50	1.0126	−0.5189	0.6751	0.013

$$A(n=\infty)=0.308\,855, \quad B(n=\infty,\eta=0.0)=3.0,$$

$$\mathrm{erf}(\eta)=\frac{2}{\sqrt{\pi}}\int_0^{\eta} e^{-t^2}\,dt.$$

The above values of A and B are numerical values. For other values of n, no simplified analytical expression can be obtained, and the integration in Eqs. (33) needs to be done numerically.

It is well known that the viscosity μ of an ideal gas is a function only of temperature, of the form[2,4]

$$\mu(T)=\mu_0\left(\frac{T}{T_0}\right)^{\omega}, \tag{35}$$

μ_0, the viscosity at the reference temperature T_0, can be used to determine $\hat{\nu}_0(n)$ in Eq. (9), and ω is a positive number of order 1. From Eqs. (9), (30), and (35) we see that

$$\omega=\frac{n+3}{2(n-1)}. \tag{36}$$

Table II gives numerical results for the Prandtl number, Eq. (30), for several values of n. It is seen that in order to obtain Pr=2/3, the coefficient b should be slightly smaller than (−0.5), which is the lower limit of this new kinetic model, to ensure the matrix ε_{ij} is positive definite. In the application of this new kinetic model, b will be chosen as (−0.5), and the Prandtl number will be close to 2/3 (for Maxwell molecules, $b=-0.5$ gives Pr=2/3). Therefore, our requirement that the physically meaningful expression of VDCF, Eqs. (9) and (32), is used and the transport coefficients are correctly predicted simultaneously, is met in this new kinetic model.

When $\nu(C)$ is not constant, and $b=0$ (which implies $\varepsilon_{ij}=\varepsilon\delta_{ij}$), the new kinetic model reduces to the $\nu(C)$-BGK model. When $\nu(C)$ is constant (therefore $\gamma_i=\hat{\gamma}_i=0$ from Eqs. (28), which is exactly true for the Maxwell molecules), this new kinetic model reduces to the ES-BGK model.

At last, we consider the H theorem for this new kinetic model. Since the explicit expression for a, Γ, and $\boldsymbol{\gamma}$ cannot be given for general situations, the H theorem is hard to prove in general, and our attempts were not successful so far. When small Knudsen numbers are considered, the H theorem is indeed satisfied. In these specific situations, one obtains from Eq. (28)

$$\begin{aligned}\ln f \cong \ln f_{\mathrm{M}} &+ \frac{b\sigma_{ij}}{2pRT}C_iC_j \\ &+ \frac{8}{3\sqrt{\pi}}\frac{C_i}{T}\frac{\partial T}{\partial x_i}\int \frac{e^{-\eta^2}\eta^4(\eta^2-5/2)}{\nu}d\eta - \frac{1}{\nu}\frac{C_iC_j}{RT}\frac{\partial u_{<i}}{\partial x_{j>}} \\ &- \frac{1}{\nu}\frac{C_i}{T}\frac{\partial T}{\partial x_i}\left(\frac{C^2}{2RT}-\frac{5}{2}\right), \\ S_m=\nu(f_N-f)=f_{\mathrm{M}}&\left[\frac{C_iC_j}{RT}\frac{\partial u_{<i}}{\partial x_{j>}}+\frac{C_i}{T}\frac{\partial T}{\partial x_i}\left(\frac{C^2}{2RT}-\frac{5}{2}\right)\right].\end{aligned} \tag{37}$$

Then, utilizing Eqs. (4) and (30), and after some manipulations (see Ref. 5 for details), the production of entropy to the first order is in fact the well-known expression for the Navier–Stokes–Fourier equations, viz.,

$$\begin{aligned}\chi=&\frac{8kp}{3\sqrt{\pi}T^2}\left(\frac{\partial T}{\partial x_i}\right)^2\int\frac{e^{-\eta^2}\eta^4(\eta^2-5/2)^2}{\nu}d\eta \\ &+\rho\left(\frac{\partial u_{<i}}{\partial x_{j>}}\right)^2\left(\frac{2b\mu}{p}+\frac{32}{15\sqrt{\pi}}\int\frac{e^{-\eta^2}\eta^6}{\nu}d\eta\right) \\ &=k\cdot\left[\frac{\kappa}{RT^2}\left(\frac{\partial T}{\partial x_i}\right)^2+\frac{2\mu\rho}{p}\left(\frac{\partial u_{<i}}{\partial x_{j>}}\right)^2\right]\geqslant 0.\end{aligned} \tag{38}$$

VI. MIEUSSENS'S DISCRETE VELOCITY MODEL

In the one-dimensional shock waves, flow is along the x direction in an x-y-z Cartesian frame. In the planar Couette flow problem, there are two parallel infinite plates in the y-z plane (one plate is fixed, while the other plate is moving with a certain speed in the y direction), and the direction perpendicular to the plates is the x direction. The flow in the planar Couette flow is along the y direction. Therefore, macroscopic variables in both situations vary only in the x direction.

The numerical method we use here is based on the explicit scheme of Mieussens's DVM. We will briefly recall the main ideas of this method and give some remarks related to situations considered here; for a complete description the reader is referred to Refs. 5, 11, and 23–25.

A. Introduction of explicit scheme

The finite volume method is used in the discretization. The space variable x is discretized on a uniform grid defined by nodes (centers of finite volumes) $x_i=(i-1)\Delta x+x_1$, where $i=1,\cdots,I$, $\Delta x=L/I$, L is the domain width, and I is the total number of position points. Microscopic particle velocities are discretized (note that they are the same for any position point and time t_n which is the time after n time steps) as, e.g., in the x direction,

$$c_x^{j_1}=c_x^1+(j_1-1)\Delta c_x,\quad c_x^1=c_{x,\min},\quad c_x^{J_1}=c_{x,\max},$$
$$j_1=1,\cdots,J_1,\quad \Delta c_x=\frac{c_{x,\max}-c_{x,\min}}{J_1-1}. \tag{39}$$

The total number of discrete velocities at one position is $J_1J_2J_3$. In the following, a dense notation is used, e.g.,

$$f(x_i,t_n,c_x^{j_1},c_y^{j_2},c_z^{j_3})=f(x_i,t_n,\mathbf{c}_j)=f_{i,j_1,j_2,j_3}^n=f_{i,j}^n. \tag{40}$$

Since the microscopic velocities are discrete, macroscopic variables, which are defined by continuous integrals of f over the velocity space [e.g., Eqs. (2)], must be replaced by discrete sums on the velocity grid. For example, mass density ρ, x component of velocity u_x, and x-y component of trace-free pressure tensor σ_{xy} will be computed as

$$\rho_i^n=\sum_{j_1=1}^{J_1}\sum_{j_2=1}^{J_2}\sum_{j_3=1}^{J_3}f_{i,j_1,j_2,j_3}^n\,\Delta c_x\,\Delta c_y\,\Delta c_z=\sum_{j=1}^{J}f_{i,j}^n\Delta\mathbf{c},$$
$$u_{x,i}^n=\frac{\sum_{j=1}^{J}c_x^{n,j_1}f_{i,j}^n\,\Delta\mathbf{c}}{\rho_i^n}, \tag{41}$$
$$\sigma_{xy,i}^n=p_{xy,i}^n=\sum_{j_1=1}^{J_1}\sum_{j_2=1}^{J_2}\sum_{j_3=1}^{J_3}C_{x,i}^{n,j_1}C_{y,i}^{n,j_2}f_{i,j_1,j_2,j_3}^n\,\Delta c_x\,\Delta c_y\,\Delta c_z$$
$$=\sum_{j=1}^{J}(c_x^{n,j_1}-u_{x,i}^n)(c_y^{n,j_2}-u_{y,i}^n)f_{i,j}^n\,\Delta\mathbf{c}.$$

The discretized kinetic equation based on an explicit finite volume scheme is

$$f_{i,j}^{n+1}=f_{i,j}^n-\frac{\Delta t_n}{\Delta x}(F_{i+1/2,j}^n-F_{i-1/2,j}^n)-\Delta t_n\,\nu_{i,j}^n(f_{i,j}^n-f_{\mathrm{ref},i,j}^n), \tag{42}$$

where Δt_n is the n^{th} time step (will be discussed in Sec. VI D), $\nu_{i,j}^n$ is the discrete collision frequency, and a Helen Yee's second-order flux expression[23,34] is applied to obtain the numerical fluxes $F_{i\pm1/2,j}^n$.

An iterative technique must be applied to obtain the solution at steady state, which in fact is what we are interested in.

B. Discrete collision frequency

The discrete dimensionless collision frequency $\hat{\nu}$, corresponding to Eq. (10) for the continuous situation, is defined as

$$\hat{\nu}_{i,j}^n=\frac{\mu_i^n}{p_i^n}\nu_{i,j}^n. \tag{43}$$

For the general ES-BGK model (which reduces to the BGK model for $b=0$, and gives $\mathrm{Pr}=2/3$ when $b=-0.5$),

$$\hat{\nu}_{\mathrm{ES},i,j}^n=\frac{1}{1-b}. \tag{44}$$

For the $\nu(C)$-BGK model, there are several expressions for $\hat{\nu}(\eta)$ presented in Ref. 9 that give the proper Prandtl number $\mathrm{Pr}=2/3$, but in this work we only consider

$$\hat{\nu}_{i,j}^n=a_i^n[1.0+\gamma_i^n(\eta_{i,j}^n)^2]. \tag{45}$$

The two coefficients a_i^n and γ_i^n in the discretized $\nu(C)$-BGK model are obtained from the following conditions, which are, in fact, the discrete form of Eqs. (19),[5]

$$\frac{4}{15\pi^{3/2}}\sum_{j=1}^{J}\frac{(\eta_{i,j}^n)^4}{\hat{\nu}_{i,j}^n}\exp[-(\eta_{i,j}^n)^2]\Delta\boldsymbol{\eta}_{i,j}^n=1,$$
$$\frac{8}{45\pi^{3/2}}\sum_{j=1}^{J}\frac{(\eta_{i,j}^n)^2((\eta_{i,j}^n)^2-5/2)^2}{\hat{\nu}_{i,j}^n}\exp[-(\eta_{i,j}^n)^2]\Delta\boldsymbol{\eta}_{i,j}^n=1, \tag{46}$$

where $\Delta\boldsymbol{\eta}_{i,j}^n=\Delta\eta_{i,j_1}^n\,\Delta\eta_{i,j_2}^n\,\Delta\eta_{i,j_3}^n=\Delta\mathbf{c}/(2RT_i^n)^{3/2}$. These conditions are solved by the Newton–Raphson (N–R) algorithm[35] (also known as the Newton method with a backtracking line search[36]).

For the new kinetic model, corresponding to Eq. (32) for the continuous situation, we have the following expression for the discrete dimensionless collision frequency:

$$\hat{\nu}(\tilde{n},\eta_{i,j}^n)=\frac{1}{1-b}\frac{16}{15\sqrt{\pi}}\cdot A(\tilde{n})\cdot B(\tilde{n},\eta_{i,j}^n), \tag{47}$$

with

$$A(\tilde{n})=\sum_{j=1}^{J}\frac{(\eta_{i,j}^n)^4\exp[-(\eta_{i,j}^n)^2]}{4\pi B(\tilde{n},\eta_{i,j}^n)}\Delta\boldsymbol{\eta}_{i,j}^n,$$
$$B(\tilde{n},\eta_{i,j}^n)=\int_{\xi=0}^{\infty}\frac{\xi e^{-\xi^2}}{\eta_{i,j}^n}[(\xi+\eta_{i,j}^n)^{3\tilde{n}-7/\tilde{n}-1}-|\xi-\eta_{i,j}^n|^{3\tilde{n}-7/\tilde{n}-1}]d\xi.$$

Note that it is not necessary to replace the integration in the above expression for the function $B(\tilde{n},\eta_{i,j}^n)$ with discrete summation over ξ in the application, while some polynomial function of η from curve fitting instead of the original integration could be applied to compute B as a function of η to save the computational time. For the hard sphere molecules, the integration can be performed and yields simplified expressions for $\hat{\nu}(\tilde{n},\eta_{i,j}^n)$,

$$\hat{\nu}(\tilde{n}=\infty,\eta_{i,j}^n)=\frac{1}{1-b}\frac{8}{15\sqrt{\pi}}\cdot A(\tilde{n}=\infty)\cdot$$

$$B(\tilde{n}=\infty,\eta_{i,j}^n=0.0)\times\left[\exp[-(\eta_{i,j}^n)^2]+\frac{\sqrt{\pi}}{2}\left(\frac{1}{\eta_{i,j}^n}+2\eta_{i,j}^n\right)\times\mathrm{erf}(\eta_{i,j}^n)\right],$$

with $A(\tilde{n}=\infty)=0.308\,855$, $B(\tilde{n}=\infty,\eta_{i,j}^n=0.0)=3.0$, and $\mathrm{erf}(\eta_{i,j}^n)$ is the error function.

Our numerical calculations show that the Prandtl number in the $\nu(C)$-BGK model and the new kinetic model based on the above expressions [Eqs. (45)–(47)] for the dimensionless collision frequency indeed has the correct value $\mathrm{Pr}\cong 2/3$ for the discrete situation as well as for the continuous situation in all test cases.

C. Discrete reference distribution

The main feature of Mieussens's DVM is that the reference distribution function f_{ref} is not discretized directly, but determined by the discrete minimum entropy principle, which, as proved by Mieussens,[23–25] is equivalent to obtain the coefficients in the reference distribution from the discrete constraints of the reference distribution [e.g., Eq. (48) below for the new kinetic model]. This implies that values of coefficients in the discrete reference distribution are not strictly identical to those in the continuous situation. In fact, if we choose values of coefficients directly from the continuous case, which was called a "natural approximation" by Mieussens,[23,24] the conservation laws and dissipation of entropy are not strictly satisfied in the discrete case.[23,24] The discrete constraints are solved through the N–R algorithm[35] here and also in Mieussens's work.[11,23,24] Since a nonlinear system is easier and more robust to be solved when magnitudes of the equations are the same, dimensionless quantities are used in the code. The discrete dimensionless reference distribution $F_{\mathrm{ref},i,j}^n$ is defined such that

$$f_{\mathrm{ref},i,j}^n=F_{\mathrm{ref},i,j}^n\frac{\rho_i^n}{\Delta\mathbf{c}}. \tag{48}$$

Expressions for $F_{\mathrm{ref},i,j}^n$, discrete constraints to determine coefficients for all kinetic models, and detailed application of the N–R algorithm in solving the constraints in the shock waves and Couette flow can be found in Refs. 5 and 11. Here only $F_{N,i,j}^n$ and its discrete constraints of the new kinetic model for shock waves are shown to save the space.

For the new kinetic model in the shock waves, the discrete dimensionless reference distribution is

$$F_{N,i,j}^n=a_{N,i}^n\exp(-\Gamma_{N,i}^n\{\Gamma_{\mathrm{ES},xx,i}^n(\eta_{i,j_1}^n)^2+\Gamma_{\mathrm{ES},yy,i}^n\times[(\eta_{i,j_2}^n)^2+(\eta_{i,j_3}^n)^2]\}+\gamma_{N,i}^n\eta_{i,j_1}^n), \tag{49}$$

and the conditions to determine the three coefficients, $a_{N,i}^n$, $\Gamma_{N,i}^n$, and $\gamma_{N,i}^n$ (Note: coefficients $\Gamma_{\mathrm{ES},xx,i}^n$ and $\Gamma_{\mathrm{ES},yy,i}^n$ are already known from the distribution $F_{\mathrm{ES},i,j}^n$ of the ES-BGK model) are obtained from the discrete form of the conservation laws

$$\sum_{j=1}^{J}\hat{\nu}_{i,j}^n\frac{(f_{N,i,j}^n-f_{i,j}^n)}{\rho_i^n}\Delta\mathbf{c}=0,$$

$$\sum_{j=1}^{J}\hat{\nu}_{i,j}^n\eta_{i,j_1}^n\frac{(f_{N,i,j}^n-f_{i,j}^n)}{\rho_i^n}\Delta\mathbf{c}=0, \tag{50}$$

$$\sum_{j=1}^{J}\hat{\nu}_{i,j}^n(\eta_{i,j}^n)^2\frac{(f_{N,i,j}^n-f_{i,j}^n)}{\rho_i^n}\Delta\mathbf{c}=0.$$

When planar Couette flow is considered, the flow velocity perpendicular to the plates, $u_{x,i}^n$, will not be forced to be zero in the procedure, so that the flow can move along the x direction to reach steady state from some initial guess. At steady state, $u_{x,i}=0.0$ should hold, and this will be used as a criterion to see when steady state is reached. Therefore, the computation of planar Couette flow by time stepping toward steady state is in fact a two-dimensional problem when the reference distribution is computed, Of course, the time evolution of distribution, Eq. (42), is still applied for planar Couette flow, for distribution and macroscopic variables only vary in the x direction at steady and nonsteady states.

D. Boundary conditions, time step, space grid, and velocity grid

Boundary conditions used in the one-dimensional shock waves are $f_{0,j}$ and $f_{I+1,j}$ (for $f_{-1,j}^n=f_{0,j}^n=f_{0,j}$ and $f_{I+1,j}^n=f_{I+2,j}^n=f_{I+1,j}$), which are the discrete equilibrium distribution at the upstream and downstream sides. Note that $f_{I+1,j}$ are computed from the *fluxes* of mass, momentum, and energy, and *not* from mass, momentum, and energy. The same procedure was also used by Mieussens.[37] This approach to get $f_{I+1,j}$ guarantees the conservation of fluxes at the discrete level, while downstream density ρ_{I+1}, velocity u_{I+1}, and temperature T_{I+1} obtained in this way will exhibit small differences to their values directly obtained from the Rankine–Hugoniot relations[38] at the continuous situation.

For the boundary conditions of planar Couette flow, the distributions at the boundaries $f_{-1,j}^n(=f_{0,j}^n)$, and $f_{I+1,j}^n(=f_{I+2,j}^n)$ change with global iteration.[5] Maxwell boundary conditions[1,2,11,39] and a classical ghost cell technique are used here.

Since an explicit scheme is used, the time step Δt_n is limited by the CFL condition,[23,24] e.g., for the shock waves, we have

$$\Delta t_n=\frac{a}{\max\limits_{i,j}(\nu_{i,j}^n)+\max\limits_{i,j_1}\left(\dfrac{|c_x^{j_1}|}{\Delta x}\right)}, \tag{51}$$

where $0<a<1.0$. $a=0.99$ is used in all computations. This restriction does not need to be applied if the implicit scheme of Mieussens's DVM is adopted.[11,23,24]

Since we wish to resolve the flow structure at the microscopic level, Δx should be chosen to be smaller than (at least

TABLE III. Quantities used in the numerical tests of kinetic models for shock waves.

Case	Domain width (m)	Mach number	Number of cells	Number of velocities	Bounds of velocities (m/s)	
					x direction	y (or z)
Sa	0.04	1.5	200	12^*11^*11	−2300, 3600	−2900, 2900
Sb	0.02	3.0	100	18^*17^*17	−3800, 5500	−4500, 4500
Sc	0.02	6.0	100	32^*30^*30	−7000, 10100	−8100, 8100

smaller than one-half in this work) some estimated mean-free path computed from boundary or initial conditions.

We follow Mieussens's choice for the bounds and step of the velocity grid,[11,23,24,37] by choosing in the x direction (similar expressions for y and z directions),

$$c_{x,\min} \leqslant \mathrm{Min}(u_{x,i} - 4\sqrt{RT_i}), \quad c_{x,\max} \geqslant \mathrm{Max}(u_{x,i} + 4\sqrt{RT_i}),$$
$$\Delta c_x \leqslant \mathrm{Min}(\sqrt{RT_i}), \quad i = 0, I+1. \tag{52}$$

The above rules for time step, step of space grid, bounds, and step of velocity grid are applied in the following numerical tests. Obviously, in order to reduce the computing time, a coarse space grid Δx and a velocity grid with small bounds [e.g., small $c_{x,\max}$ in Eqs. (39) and (52)] and large step [e.g., Δc_x in Eq. (52)] are preferred.

VII. NUMERICAL TESTS

A. Test examples

Shock waves are characterized by their upstream Mach number Ma, which is defined as

$$\mathrm{Ma} = \frac{u_U}{a}, \tag{53}$$

where u_U and $a = \sqrt{5RT_U/3}$ are the flow and sound speed at the upstream equilibrium state.

In the numerical tests for shock waves, one weak shock wave (Ma=1.5), one medium shock wave (Ma=3.0), and one strong shock wave (Ma=6.0) have been tested. There are some common parameters in the numerical tests for shock waves, which are as follows: gas molecules are modeled as ideal hard sphere molecules; the material is helium; the upstream temperature is 160.0 K; the upstream number density (defined as density over molecular mass) is 2.889E21 $1/\mathrm{m}^3$; the reference temperature T_0 is 273.0 K; viscosity at the reference temperature μ_0 is 1.86E-5 kg/m s;[40] Boltzmann's constant k is 1.381E-23 J/K; Avogadro's number N is 6.022E23 1/mol;[38] the molecular mass of helium m is 6.65E-27 kg.[41] The mean-free path at the upstream side l is 1.287 mm, based on the following definition:

$$l = \mu \frac{\sqrt{RT}}{nkT}, \tag{54}$$

where $n = \rho/m$ is the number density, and μ is the viscosity as computed from Eq. (35). For other values see Table III, which shows the situations and quantities used in the numerical tests of kinetic models for one-dimensional shock waves.

The important parameter for planar Couette flow is the Knudsen number Kn, defined as the ratio of the mean-free path l over the distance L between the two plates, $\mathrm{Kn} = l/L$. For the tests, the Knudsen numbers Kn=0.025, 0.1, 0.5, and 1.0 were used. The plate speeds were set to 300.0 m/s, 600.0 m/s, and 1000.0 m/s. Altogether, there are 12 different test situations; see Table IV for details, which shows cases and the corresponding quantities used in the numerical tests of kinetic models for planar Couette flow. There are some common parameters in the numerical tests, which are as follows: gas molecules are modeled as ideal hard sphere molecules;[42] the material is argon; the temperatures of both plates are 273.0 K; the speed of plate 1 is zero; the speed of plate 2 is chosen as indicated in Table IV; the number density at the initial state is 1.4E20 $1/\mathrm{m}^3$; the reference temperature is 273.0 K; the viscosity at the reference temperature is 1.9552E-5 kg/m s;[43] the molecular mass of argon is 6.63E-26 kg;[41] the mean-free path l from the above definition, Eq. (54), is 8.833 mm for the initial state.

For each test case, the BGK model, the ES-BGK model with $b=-0.5$ (Pr=2/3), the $\nu(C)$-BGK model, the new kinetic model with $b=-0.5$ (Pr$\cong$2/3, see Table II for details)

TABLE IV. Quantities used in the numerical tests of kinetic models for planar Couette flow.

Case	Kn	Domain width (mm)	Speed of plate (m/s)	Number of cells	Number of velocities	Bound of velocities (m/s)	
						y direction	x (or z)
Sa	0.025	353.3	300.0	100	11^*10^*10	−1100, 1400	−1100, 1100
Sc	0.1	88.33	300.0	50	11^*10^*10	−1100, 1400	−1100, 1100
Se	0.5	17.67	300.0	50	11^*10^*10	−1100, 1400	−1100, 1100
Sg	1.0	8.833	300.0	25	11^*10^*10	−1100, 1300	−1100, 1100
Si	0.5	17.67	600.0	50	13^*12^*12	−1100, 1700	−1300, 1300
Sj	0.5	17.67	1000.0	50	16^*14^*14	−1200, 2200	−1500, 1500

TABLE V. Quantities used in the numerical tests of DSMC.

Parameter	Meaning	Value for shock waves	Value for planar Couette flow
FNUM	Number of real molecules represented by each simulated molecule	1.4445E15	5.6E14
MNM	Maximum number of simulator molecules	5E6	2.5E5
DTM (s)	Time step over which the movement and collision steps are uncoupled	1E−7	3.125E−7
NIS	Number of time steps between samples	4	4
NSP	Number of samples between file updates	20	1600
NPS	Number of updates to reach steady flow	100	50
NPT	Number of file updates to completion	20000	1000
SP(1,1) (m)	Reference molecular diameter	2.19E−10	3.7758E−10
SP(3,1)	Viscosity-temperature index	0.5	0.5
SP(4,1)	The reciprocal of the VSS scattering parameter	1.0	1.0
MNC	Maximum number of cells	400	2000 for Kn=0.025; 500 for Kn=0.1; 100 for Kn=0.5; 50 for Kn=1.0
MNSC	Maximum number of subcells	4000	20000 for Kn=0.025; 5000 for Kn=0.1; 1000 for Kn=0.5; 500 for Kn=1.0

are tested. Table V shows the corresponding quantities used for the DSMC computations that are used as a benchmark in this work.[43]

B. Some notes on dealing with the results

Since there is no fixed coordinate label for the shock profile inherent to the problem,[3,11,44] all shock wave data is analyzed, shifting the curves such that, in the origin, $x=0$, of the new Cartesian frame the density takes on the arithmetic mean of the downstream and upstream values.[3,44] For the planar Couette flow, no shifting is needed since the positions of the boundaries are fixed.

Only a small part of the produced data and graphs can be shown because of limited space; for more details refer to Ref. 5, or contact the authors.

C. Steady-state analysis

Since results at steady state are what we are interested in, we need to establish whether the computational results are at steady state indeed. For the steady shock waves, the mass flux ρu_x, the momentum flux $\rho u_x^2+p_{xx}$, and the energy flux $1.5pu_x+0.5\rho u_x^3+p_{xx}u_x+q_x$, all should be constant in the whole domain. For steady planar Couette flow, the quantities $u_x=0$, p_{xx}, σ_{xy}, $u_y\sigma_{xy}+q_x$ should be constant in the whole domain.[5] Because of numerical fluctuations, the velocity perpendicular to the plates u_x will never be exactly zero in the computation, but will be very small. Therefore it makes more sense to consider the dimensionless velocity $u_x/\sqrt{RT}$ instead of u_x itself.

It was found that the final computational results we obtained are converged, stable, and indeed correspond to steady state for all tests.[5]

D. Comparison of results among kinetic models and DSMC

Results from the BGK model, the ES-BGK model, the $\nu(C)$-BGK model, and DSMC computations for one-dimensional shock waves and planar Couette flow have been compared and discussed in detail in Ref. 11. Here, only the comparison of kinetic models as related to the new kinetic models will be described. Figures 1 and 2 show velocity and temperature profiles for a shock wave at Ma=3.0 from kinetic models and DSMC. Figures 3 and 4 show density and temperature profiles for a shock wave at Ma=6.0 from kinetic models and DSMC. Figures 5 and 6 show Couette flow density and parallel heat flux profiles from kinetic models and the DSMC at situation Si in Table IV. Figures 7 and 8 show Couette flow parallel heat flux and temperature profiles from kinetic models and the DSMC at situation Sa in Table IV.

When the computational time for each iteration is considered, the new kinetic model requires the longest time, followed by the $\nu(C)$-BGK model, the ES-BGK model, and the BGK model. The time ratio of the new kinetic model to the ES-BGK model to the BGK model is about 3:2:1. Since an explicit numerical scheme, see Eq. (42), is used in this work, computational times in the tests are of the same order as those encountered in the DSMC.

For hard sphere molecules, results from the new kinetic model are located in between results from the $\nu(C)$-BGK model and results from the ES-BGK model for almost all test cases in shock waves and Couette flow, which can be seen from Figs. 1–8.

When the shape of the temperature of shock waves is considered, results from the $\nu(C)$-BGK model are the steep-

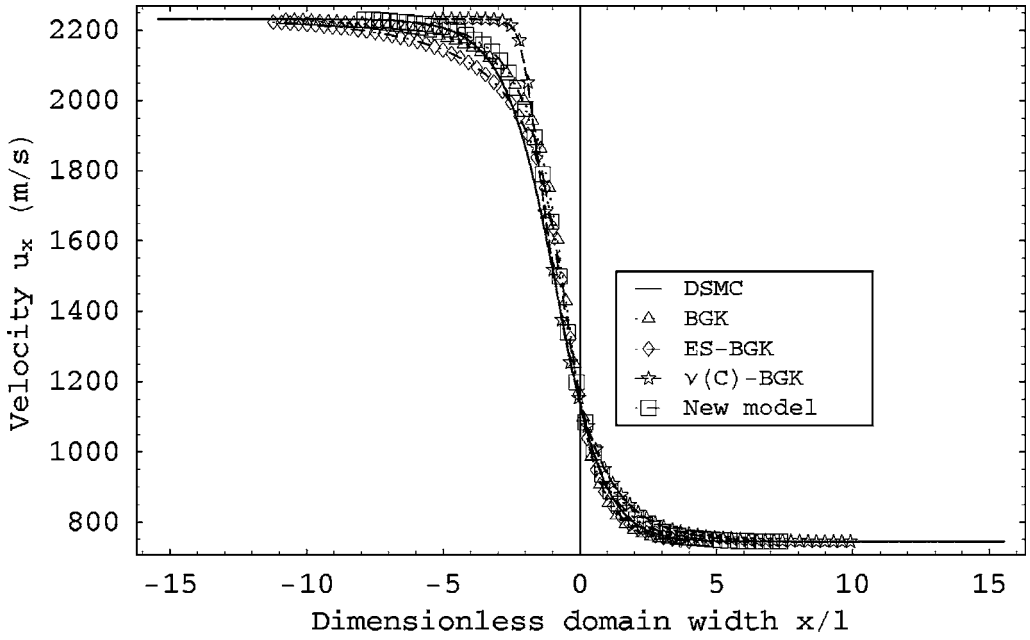

FIG. 1. Velocity profiles of shock waves at Ma=3.0.

est, while results from the ES-BGK model are the gentlest. Results from the new kinetic model lie in between these extremes, and are, in fact, closer to results from the DSMC. These two points are well exhibited in Figs. 2 and 4. (Note, in fact, the shape of density has a similar phenomenon, but not apparent, as the shape of temperature.) It can be seen from Fig. 4 that the ES-BGK model, the new kinetic models and the DSMC exhibit the overshoot phenomenon of temperature for large Mach situations (e.g., Ma=6.0), while results from the BGK model and the $\nu(C)$-BGK model do not have this phenomenon. Therefore, the new kinetic models indeed give better results for shock waves than the other kinetic models. This must be attributed to the use of the proper velocity-dependent collision frequency.

There are two main points against the application of the $\nu(C)$-BGK model for planar Couette flow. One is that for large Knudsen numbers (e.g., $\mathrm{Kn} \geqslant 0.5$), the shape of the density profile becomes too flat compared to the DSMC results. This issue can be seen from Fig. 5, and was already pointed out in Ref. 11, where it was shown that this might be due to different possibilities for choosing the Knudsen number, but most likely it is a general failure of the $\nu(C)$-BGK model.[11] Another point is that results for the parallel heat flux q_y from the $\nu(C)$-BGK model fit results from the DSMC

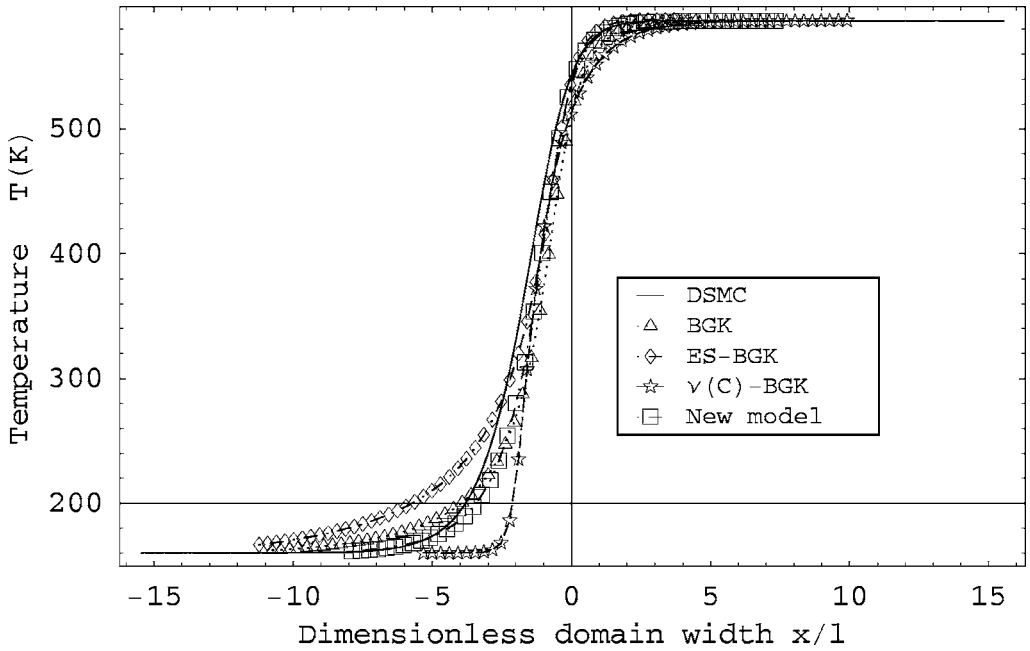

FIG. 2. Temperature profiles of shock waves at Ma=3.0.

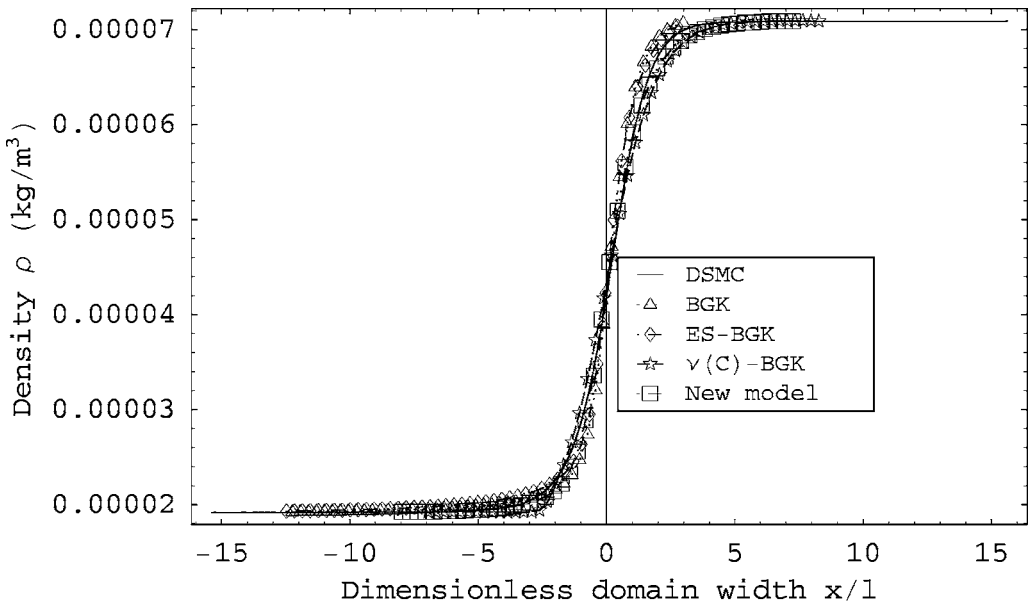

FIG. 3. Density profiles of shock waves at Ma=6.0.

worst among all kinetic models considered. For small plate velocities (which correspond to small Mach numbers), we even obtained q_y with opposite signs compared to values from the DSMC, as can be seen from Fig. 7.

Combining the above analysis about the $\nu(C)$-BGK model and the above discussion about the location of results from the new kinetic models compared to results from the ES-BGK model and the $\nu(C)$-BGK model, results from the new kinetic model are often worse than (see Figs. 5–7) results from the ES-BGK model, which reason, from the physical view, is that the equilibrium Maxwellian distribution is applied for the expression of collision frequency [Eq. (9)], which is used in the new kinetic model. Therefore, the ES-BGK model is a better choice for planar Couette flow than the new kinetic models from results and computational time.

Finally, we consider the application of the BGK model and the ES-BGK model in the planar Couette flow. For small Knudsen numbers ($\mathrm{Kn} \leqslant 0.1$), where the Prandtl number is meaningful, the ES-BGK model gives better results than the BGK model. It makes sense since the BGK model gives the wrong Prandtl number Pr=1, while Pr=2/3 in the ES-BGK model. It can be seen from Fig. 8 that the curve from the BGK model departs from the other curves, which are all similar to each other. This phenomenon can be explained from the fact that Pr=1 in the BGK model, while Pr=2/3 in other kinetic models, and Kn=0.025 is quite a small value.

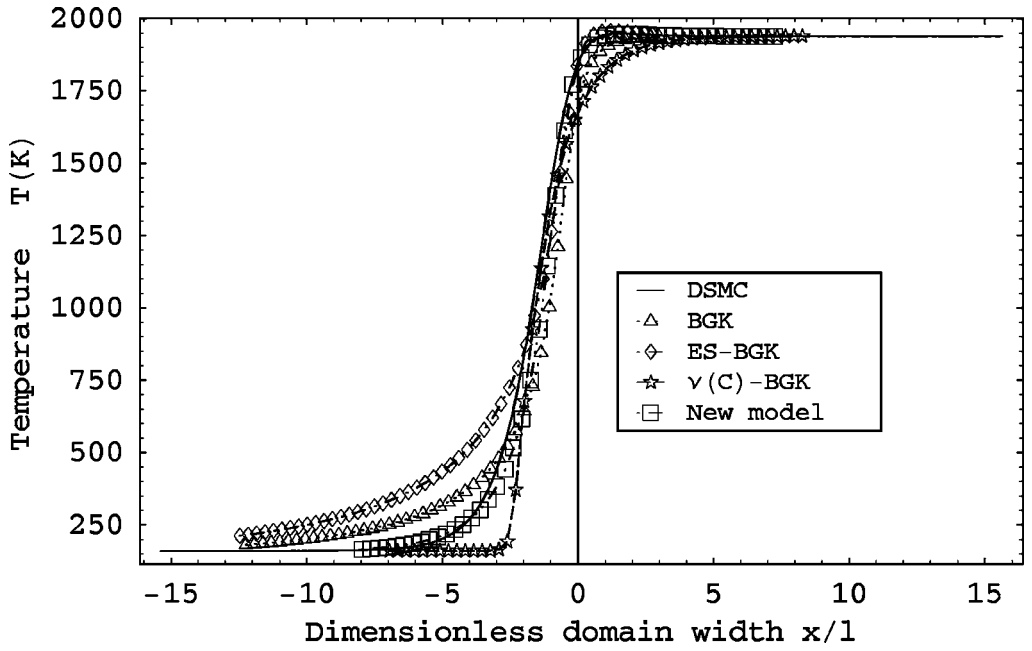

FIG. 4. Temperature profiles of shock waves at Ma=6.0.

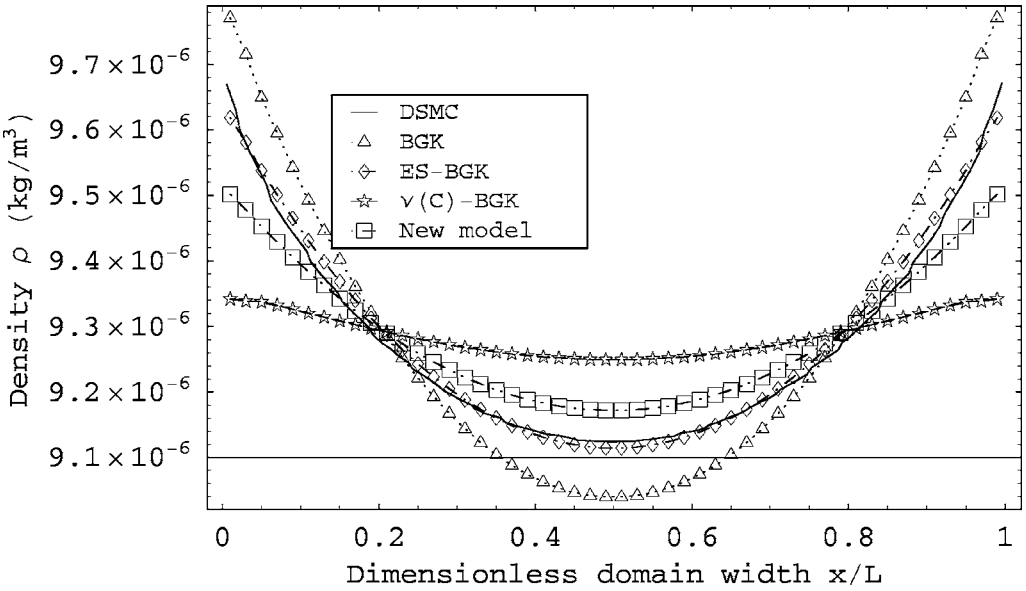

FIG. 5. Density profiles of planar Couette flow at situation Si (Kn=0.5, 600.0 m/s plate speed).

The Prandtl number is related to the collision frequency through viscosity and heat conductivity, which can be considered as weighted mean values of the collision frequency, relevant for the transport of momentum and energy. Viscosity and heat conductivity determine the flow for small Knudsen numbers, where the Navier–Stokes–Fourier equations are relevant. For large Knudsen numbers, however, details of the collision frequency, in particular its velocity dependence, become important, and this is why the results from all kinetic models differ for larger Knudsen numbers. For shock waves, the use of realistic collision frequencies leads to marked improvements as compared to models that use either a constant mean value of the collision frequency (ES-BGK model), or unrealistic velocity functions [$\nu(C)$-BGK model]. For Couette flow at larger Knudsen numbers it is realized that none of these two kinetic models gives better results than another one for all tests. Therefore, we suggest using the ES-BGK model, instead of the BGK model for further consideration of flows with the Knudsen layer, especially for small Knudsen numbers.

VIII. CONCLUSION

Several existing kinetic models—the BGK model, the ES-BGK model, the $\nu(C)$-BGK model, the Shakhov model, and the Liu model—have been described and compared, based on properties that need to be satisfied for a kinetic model. The main disadvantage of these existing kinetic mod-

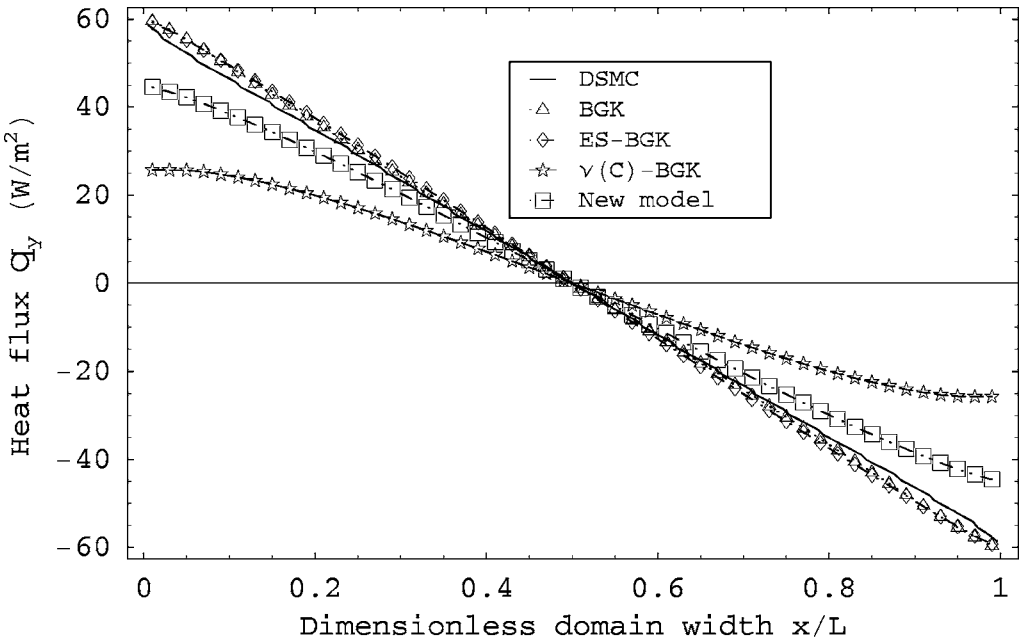

FIG. 6. Heat flux q_y profiles of planar Couette flow at situation Si (Kn=0.5, 600.0 m/s plate speed).

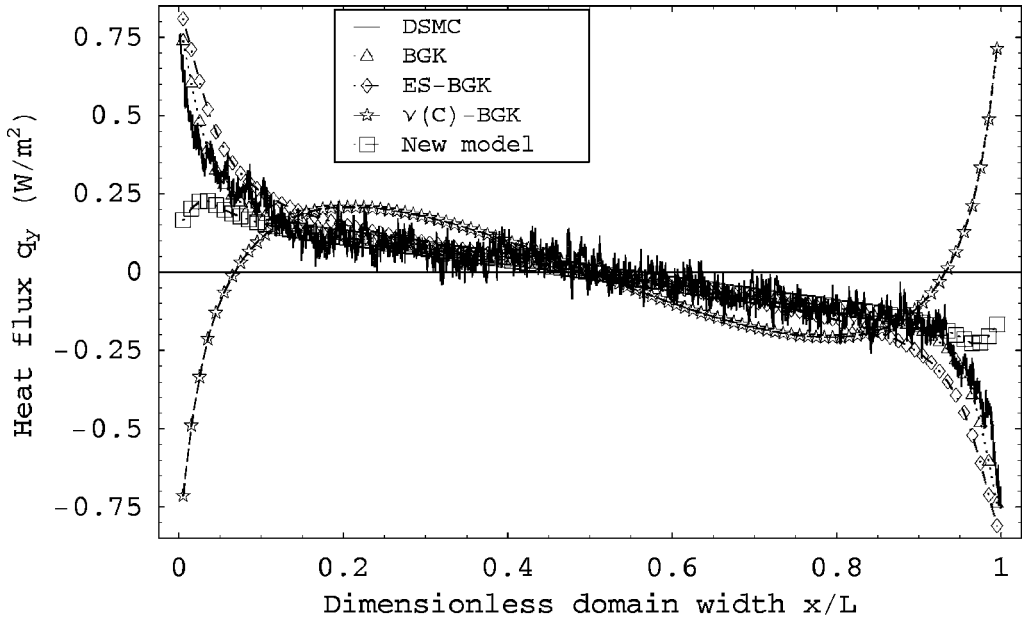

FIG. 7. Heat flux q_y profiles of planar Couette flow at situation Sa (Kn=0.025, 300.0 m/s plate speed).

els is that the physically meaningful expression of the VDCF, Eq. (9), and the proper Prandtl number $\mathrm{Pr} \cong 2/3$ cannot be reached at the same time.

In order to overcome this shortcoming, a new $\nu(C)$-ES-BGK-type kinetic model has been proposed here, which can be simplified to the ES-BGK model and the $\nu(C)$-BGK model for suitable choices of parameters. The H theorem for the new kinetic model has so far been proven only for small Knudsen numbers.

In this paper we discussed the kinetic models in principle, and examined their behavior for small Knudsen numbers, where their coefficients can be adjusted such that the models give the proper values for the relevant transport coefficients, namely viscosity and heat conductivity (and thus the proper Prandtl number). In this limit, the velocity dependence of the collision frequency is visible only in the higher level of complexity of the models, but not in the resulting equations, which are, of course, the laws of Navier–Stokes and Fourier.

However, the velocity dependence will be important in transport regimes where the Navier–Stokes and Fourier equations are not applicable, i.e., for not too small Knudsen numbers. Then, the gas must be described through the Boltzmann equation, or, alternatively, through one of the kinetic models described in this paper.

In this second part of this work, several kinetic models

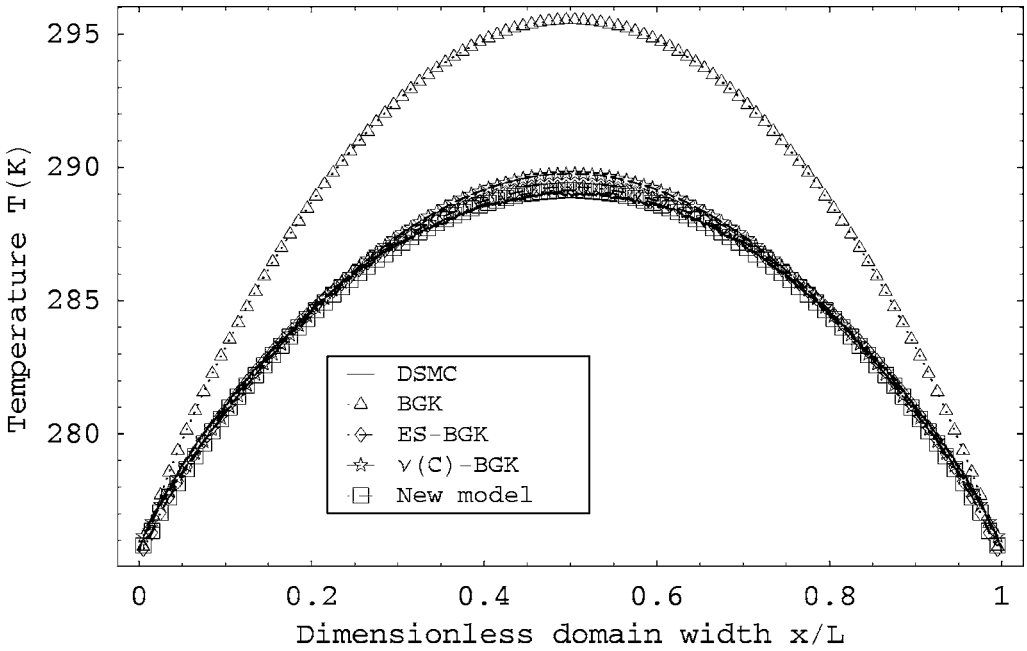

FIG. 8. Temperature profiles of planar Couette flow at situation Sa (Kn=0.025, 300.0 m/s plate speed).

are tested numerically for the situations of one-dimensional shock waves at steady state and planar Couette flow at steady state. The models considered were the BGK model, the ES-BGK model, the $\nu(C)$-BGK model, and the new kinetic model. Computational results from the kinetic models are compared to results obtained from the DSMC calculation, which serves as a benchmark.

For hard sphere molecules, results from the new kinetic model are located in between results from the ES-BGK model and the $\nu(C)$-BGK model, and are closer to DSMC results than these.

For the shock wave problem, the new kinetic model gives the best agreement to the DSMC simulation (e.g., standard average relative errors for density, velocity, temperature, and pressure are smaller than 0.06, even for Ma=6.0 when results from the new kinetic model are compared to results from the DSMC[5]); while for Couette flow the ES-BGK model is the best choice, since the standard average relative errors density, velocity, temperature, and pressure are smaller than 0.035 for all test situations when results from the ES-BGK model are compared to results from the DSMC.[5] The $\nu(C)$-BGK model gives results of insufficient accuracy in both shock waves and Couette flow; therefore, it is not suggested to be used to model rarefied gas flows.

ACKNOWLEDGMENTS

This research was supported by the Natural Sciences and Engineering Research Council (NSERC) of Canada. The authors wish to thank Dr. Luc Mieussens for many helpful discussions on his discrete velocity model and Adam Schuetze for the DSMC computations. Y.Z. would also like to thank Professor Jason Reese in the University of Strathclyde and the Leverhulme Trust in the UK for current support that enabled him to write the paper.

[1] H. Struchtrup, *Macroscopic Transport Equations for Rarefied Gas Flows—Approximation Methods in Kinetic Theory*, Interaction of Mechanics and Mathematics Series (Springer, Heidelberg, 2005).
[2] M. N. Kogan, *Rarefied Gas Dynamics* (Plenum, New York, 1969).
[3] C. Cercignani, *Rarefied Gas Dynamics: From Basic Concepts to Actual Calculations* (Cambridge University Press, Cambridge, 2000).
[4] V. Garzo and A. Santos, *Kinetic Theory of Gases in Shear Flows* (Kluwer Academic, Dordrecht, 2003).
[5] Y. Zheng, "Analysis of kinetic models and macroscopic continuum equations for rarefied gas dynamics," Ph.D. thesis, Department of Mechanical Engineering, University of Victoria, Canada, 2004.
[6] P. L. Bhatnagar, E. P. Gross, and M. Krook, "A model for collision processes in gases. I: small amplitude processes in charged and neutral one-component systems," Phys. Rev. **94**, 511 (1954).
[7] J. Lowell and H. Holway, "New statistical models for kinetic theory: methods of construction," Phys. Fluids **9**, 1658 (1966).
[8] P. Andries and B. Perthame, "The ES-BGK model equation with correct Prandtl number," AIP Conf. Proc. **585**, 30 (2001).
[9] Y. Zheng and H. Struchtrup, "Burnett equations for the ellipsoidal statistical BGK model," Continuum Mech. Thermodyn. **16**, 97 (2004).
[10] H. Struchtrup, "The BGK-model with velocity-dependent collision frequency," Continuum Mech. Thermodyn. **9**, 23 (1997).
[11] L. Mieussens and H. Struchtrup, "Numerical comparison of BGK-models with proper Prandtl number," Phys. Fluids **16**, 2797 (2004).
[12] F. Bouchut and B. Perthame, "A BGK model for small Prandtl number in the Navier-Stokes approximation," J. Stat. Phys. **71**, 191 (1993).
[13] L. B. Barichello, A. C. R. Bartz, M. Camargo, and C. E. Siewert, "The temperature-jump problem for a variable collision frequency model," Phys. Fluids **14**, 382 (2002).
[14] C. Ceicignani, "The method of elementary solutions for kinetic models with velocity-dependent collision frequency," Ann. Phys. **40**, 469 (1966).
[15] V. Garzó, "Perturbative solution of the BGK equation for very hard particle interaction," Mol. Phys. **63**, 517 (1988).
[16] J. J. Brey and A. Santos, "Solution of the BGK model kinetic equation for very hard particle interaction," J. Stat. Phys. **37**, 123 (1984).
[17] E. M. Shakhov, "Generalization of the Krook kinetic relaxation equation," Fluid Dyn. **3**, 95 (1968).
[18] F. Sharipov and V. Seleznev, "Data on internal rarefied gas flows," J. Phys. Chem. Ref. Data **27**, 657 (1998).
[19] G. Liu, "A method for constructing a model form for the Boltzmann equation," Phys. Fluids A **2**, 277 (1990).
[20] V. Garzo and M. L. d. Haro, "Kinetic model for heat and momentum transport," Phys. Fluids **6**, 3787 (1994).
[21] H. Babovsky and R. Illner, "A convergence proof for Nanbu's simulation method for the full Boltzmann equation," SIAM (Soc. Ind. Appl. Math.) J. Numer. Anal. **26**, 45 (1989).
[22] G. A. Bird, *Molecular Gas Dynamics and the Direct Simulation of Gas Flows* (Oxford Science, Oxford, 1994).
[23] L. Mieussens, "Discrete-velocity models and numerical schemes for the Boltzmann-BGK equation in plane and axisymmetric geometries," J. Comput. Phys. **162**, 429 (2000).
[24] L. Mieussens, "Discrete velocity model and implicit scheme for the BGK equation of rarefied gas dynamics," Math. Models Meth. Appl. Sci. **10**, 1121 (2000).
[25] L. Mieussens, "Convergence of a discrete-velocity model for the Boltzmann-BGK equation," Comput. Math. Appl. **41**, 83 (2001).
[26] In this paper, the term "distribution function" always refers to the mass distribution function, which is the mass of one microscopic particle m times the number distribution function (or phase density) that is also often used in kinetic theory.
[27] C. D. Levermore, "Entropy-based moment closures for kinetic equations," Transp. Theory Stat. Phys. **26**, 591 (1997).
[28] P. Le Tallec, "A hierarchy of hyperbolic models linking Boltzmann to Navier Stokes equations for polyatomic gases," Z. Angew. Math. Mech. **80**, 779 (2000).
[29] J. O. Hirschfelder, C. F. Curtiss, and R. B. Bird, *Molecular Theory of Gases and Liquids* (Wiley, New York, 1954).
[30] S. Chapman and T. G. Cowling, *The Mathematical Theory of Non-Uniform Gases*, 3rd ed. (Cambridge Univerisity Press, Cambridge, 1970).
[31] J. W. Dufty and A. Baskaran, "Gaussian kinetic model for granular gases," Phys. Rev. E **69**, 051301 (2004).
[32] C. Ceicignani, "Knudsen layers: theory and experiment," in *Recent Developments in Theoretical and Experimental Fluid Mechanics*, edited by U. Muller, K. G. Rosner, and B. Schmidt (Springer, Berlin, 1979), pp. 187–195.
[33] In Ref. 5, another $\nu(C)$-ES-BGK-type kinetic model with ten unknown coefficients, which, in fact, is a generalization of the one [Eqs. (25)] discussed in this paper, is also constructed. The description about that model is omitted in this paper, for there is limited space for a paper and its performance is not good as the one discussed in the paper.
[34] H. C. Yee, "Construction of explicit and implicit symmetric TVD schemes and their applications," J. Comput. Phys. **68**, 151 (1987).
[35] W. H. Press, B. P. Flannery, S. A. Teukolsky, and W. T. Vetterling, *Numerical Recipes* (Cambridge University Press, Cambridge, 1986).
[36] J. E. Dennis and R. B. Schnabel, *Numerical Methods for Unconstrained Optimization and Nonlinear Equations* (Prentice–Hall, Englewood Cliffs, NJ, 1983).
[37] L. Mieussens (private communication, Toulouse, France, 2003).
[38] W. G. Vincenti and C. H. Kruger, Jr., *Introduction to Physics Gas Dynamics* (Wiley, New York, 1965).
[39] H. Struchtrup, "Kinetic schemes and boundary conditions for moment equations," ZAMP **51**, 346 (2000).
[40] G. C. Pham-Van-Diep, D. A. Erwin, and E. P. Muntz, "Testing continuum descriptions of low-Mach-number shock structures," J. Fluid Mech. **232**, 403 (1991).
[41] R. B. Bird, W. E. Stewart, and E. N. Lightfoot, *Transport Phenomena*, 2nd ed. (Wiley, New York, 2002).
[42] Maxwell molecules have also been applied in the tests for planar Couette flow in Ref. 5, whose results have been omitted in this paper, for the new

kinetic model is identical with the classical ES-BGK model for the Maxwell molecules.
[43] A. Schuetze, "Direct simulation by Monte Carlo modeling Couette flow using dsmc1as.f: A user's manual," Report, Department of Mechanical Engineering, University of Victoria, 2003.
[44] T. Ohwada, "Structure of normal shock waves: Direct numerical analysis of the Boltzmann equation for hard-sphere molecules," Phys. Fluids A **5**, 217 (1993).